

RESEARCH ARTICLE

10.1002/2016JD025471

Special Section:

Studies of Emissions and Atmospheric Composition, Clouds and Climate Coupling by Regional Surveys, 2013 (SEAC4RS)

Key Points:

- Observations are reported for growth factor (GF) and $f(\text{RH})$ values below 1 in multiple regions using three instruments
- GF and $f(\text{RH})$ values less than 1 are observed in biomass burning plumes, organic-rich particles, and wintertime in an urban area
- $f(\text{RH})$ increases as a function of effective particle density with the majority of values below 1 coincident with density $< 1.2 \text{ g cm}^{-3}$

Supporting Information:

- Supporting Information S1
- Figure S1

Correspondence to:

A. Sorooshian,
armin@email.arizona.edu

Citation:

Shingler, T., et al. (2016), Ambient observations of hygroscopic growth factor and $f(\text{RH})$ below 1: Case studies from surface and airborne measurements, *J. Geophys. Res. Atmos.*, 121, 13,661–13,677, doi:10.1002/2016JD025471.

Received 6 JUN 2016

Accepted 1 NOV 2016

Accepted article online 7 NOV 2016

Published online 23 NOV 2016

Ambient observations of hygroscopic growth factor and $f(\text{RH})$ below 1: Case studies from surface and airborne measurements

Taylor Shingler^{1,2,3}, Armin Sorooshian^{1,4}, Amber Ortega^{1,5}, Ewan Crosbie^{2,3}, Anna Wonaschütz⁶, Anne E. Perring^{7,8}, Andreas Beyersdorf³, Luke Ziemba³, Jose L. Jimenez^{8,9}, Pedro Campuzano-Jost^{8,9}, Tomas Mikoviny¹⁰, Armin Wisthaler^{10,11}, and Lynn M. Russell¹²

¹Department of Chemical and Environmental Engineering, University of Arizona, Tucson, Arizona, USA, ²NASA Langley Research Center, Hampton, Virginia, USA, ³Universities Space Research Association, Columbia, Maryland, USA, ⁴Department of Hydrology and Atmospheric Sciences, University of Arizona, Tucson, Arizona, USA, ⁵Now at Air Pollution Control Division, Colorado Department of Public Health and Environment, Denver, Colorado, USA, ⁶Faculty of Physics, University of Vienna, Vienna, Austria, ⁷NOAA Earth System Research Laboratory, Boulder, Colorado, USA, ⁸Cooperative Institute for Research in Environmental Sciences, University of Colorado Boulder, Boulder, Colorado, USA, ⁹Department of Chemistry and Biochemistry, University of Colorado Boulder, Boulder, Colorado, USA, ¹⁰Department of Chemistry, University of Oslo, Oslo, Norway, ¹¹Institute for Ion Physics and Applied Physics, University of Innsbruck, Innsbruck, Austria, ¹²Scripps Institution of Oceanography, University of California, San Diego, California, USA

Abstract This study reports a detailed set of ambient observations of optical/physical shrinking of particles from exposure to water vapor with consistency across different instruments and regions. Data have been utilized from (i) a shipboard humidified tandem differential mobility analyzer during the Eastern Pacific Emitted Aerosol Cloud Experiment in 2011, (ii) multiple instruments on the NASA DC-8 research aircraft during the Studies of Emissions, Atmospheric Composition, Clouds and Climate Coupling by Regional Surveys in 2013, and (iii) the Differential Aerosol Sizing and Hygroscopicity Spectrometer Probe during ambient measurements in Tucson, Arizona, during summer 2014 and winter 2015. Hygroscopic growth factor (ratio of humidified-to-dry diameter, $\text{GF} = D_{p,\text{wet}}/D_{p,\text{dry}}$) and $f(\text{RH})$ (ratio of humidified-to-dry scattering coefficients) values below 1 were observed across the range of relative humidity (RH) investigated (75–95%). A commonality of observations of GF and $f(\text{RH})$ below 1 in these experiments was the presence of particles enriched with carbonaceous matter, especially from biomass burning. Evidence of externally mixed aerosol, and thus multiple GFs with at least one $\text{GF} < 1$, was observed concurrently with $f(\text{RH}) < 1$ during smoke periods. Possible mechanisms responsible for observed shrinkage are discussed and include particle restructuring, volatilization effects, and refractive index modifications due to aqueous processing resulting in optical size modification. To further investigate ambient observations of GFs and $f(\text{RH})$ values less than 1, it is recommended to add an optional prehumidification bypass module to hygroscopicity instruments, to preemptively collapse particles prior to controlled RH measurements.

1. Introduction

Aerosol-water interactions influence how ambient particles scatter solar radiation, act as cloud condensation nuclei (CCN), and deposit to surfaces, including in the human respiratory system [Dua and Hopke, 1996]. These interactions are important to account for in remote sensing retrievals of aerosol particles due to artifacts that result from aerosol swelling in moist areas such as next to clouds, in addition to using retrieved columnar aerosol data to estimate fine particulate matter ($\text{PM}_{2.5}$) [Kim et al., 2015]. Representing the ability to take up water vapor at fixed relative humidity (RH), hygroscopicity is a property of particles dependent on size and composition. Improving the understanding of aerosol hygroscopicity will improve predictability of future climate, as aerosol interactions with water vapor and clouds are the largest source of uncertainty in estimates of total anthropogenic radiative forcing [Intergovernmental Panel on Climate Change, 2013].

In order to study aerosol hygroscopicity in the atmosphere, a number of instruments have been developed. Traditionally, the humidified tandem differential mobility analyzer (HTDMA [Liu, 1978; Rader and McMurry, 1986]) has been used for size-resolved, subsaturated aerosol water uptake measurements; however, the long sampling time required to scan through a complete size distribution is impractical for aircraft applications. The Differential Aerosol Sizing and Hygroscopicity Spectrometer Probe (DASH-SP, Brechtel Mfg. Inc.)

[Sorooshian *et al.*, 2008a] is a newer instrument designed specifically for aircraft-based, rapid, size-resolved measurements of aerosol subsaturated hygroscopicity using optical particle counters (OPCs) in place of a second differential mobility analyzer (DMA) in the HTDMA. When comparing the HTDMA and DASH-SP, the final humidified particle size distributions are based on different measurement principles including electrical mobility and an optically based algorithm, respectively. Both instruments quantify hygroscopic growth factor (GF), defined as the ratio of humidified particle diameter to a fixed, single diameter at dry conditions ($GF = D_{p,wet}/D_{p,dry}$). Nephelometer-based instruments quantify hygroscopicity for bulk aerosol using the parameter $f(RH)$, which is the ratio of light scattering from all particle sizes in humid (typically RH of ~80%) versus dry conditions (typically RH less than 20%). While the nephelometer-based instruments are rapid and suited for aircraft measurements, key differences with the previous two instruments are that $f(RH)$ data are not size resolved and have limitations in terms of probing RHs above 85% [Kreidenweis and Asa-Awuku, 2014].

While extensive research has reported on GF and $f(RH)$ values extending from unity (i.e., no growth upon hydration) to higher values, only studies based on laboratory work, summarized below, have reported hygroscopic growth less than 1, suggestive of particle size shrinkage upon hydration. Hygroscopic GFs below 1 result when the humidified diameter is less than the original dry diameter ($D_{p,dry}$) or when the total scattering of humidified ambient air is less than dried ambient air. Hygroscopicity can be expressed in terms of a single parameter, kappa (κ), developed by Petters and Kreidenweis [2007], which is related to GF as shown by the approximation in equation (1). The κ model does not allow for values of $\kappa < 0$ (as a result of $GF < 1$), and therefore, κ will be referred to here as an effective κ (κ_e).

$$[GF]^3 = 1 + \kappa \left(\frac{\frac{RH}{100\%}}{1 - \frac{RH}{100\%}} \right). \quad (1)$$

Numerous explanations for $GF < 1$ have been presented in past laboratory-based studies. They include surface-active organic species [Petters and Kreidenweis, 2013], slightly soluble organic compounds [Petters and Kreidenweis, 2008], and elemental carbon restructuring [Tritscher *et al.*, 2011]. The majority of the literature has been devoted to particle restructuring. For example, flame-generated soot from diesel and propane combustion shows evidence of particle restructuring at an RH as low as 35% [Henning *et al.*, 2012]. Using a similar particle source, Weingartner *et al.* [1997] concluded that the restructuring process was still occurring and had not reached steady state with RH up to 80%. Another study showed that soot restructuring in acetylene and ethylene burner emissions occurs upon water evaporation and is likely attributed to capillary effects [Ma *et al.*, 2013]. Hydrophilic soot particles collapse into globules with increased RH [Mikhailov *et al.*, 2006], yet when diluted with warm particle-free air, their fractal structure stays intact until humidification at $RH > 90\%$ [Rissler *et al.*, 2005]. Although not directly related to hygroscopic growth instruments, soot from a propane diffusion flame has also been shown to undergo morphological transformations, from chain-like to compact structure, which is explained by Coulomb interactions between parts of the aggregated soot particle [Onischuk *et al.*, 2003].

Nonburner emitted particles also demonstrate restructuring behavior. Jimenez *et al.* [2003] observed that iodine oxide particles formed under dry conditions were fractal agglomerates but became more compact and more dense at higher RHs. There is evidence that biomass burning combustion particles of 100 nm or larger are more readily restructured upon hydration [Martin *et al.*, 2013]. The decrease in mobility diameter upon humidification is more pronounced for larger particles [Pagels *et al.*, 2009]. Weingartner *et al.* [1995] found that organic particles above 100 nm shrank into a more compact structure at $RH = 90\%$ due to capillary forces induced on any asymmetrical part of the structure. Lewis *et al.* [2009] reported that wood smoke from combustion of chamise and palmetto collapsed to a more spherical and compact shape upon exposure to high RH, while smoke from ponderosa pine, with lower inorganic content, did not show this behavior. Mochida and Kawamura [2004] showed that the GF of lignin pyrolysis products (4-hydroxybenzoic acid and vanillic and syringic acids) were just below 1.0 (>0.95) up to an RH of 95%, which they attributed to either restructuring or, potentially, evaporation of organics in the HTDMA. Beaver *et al.* [2008] showed that 4-hydroxybenzoic acid exhibited $f(RH)$ values below unity with the lowest values for the smallest optical effective diameter examined in their experiments ($f(RH = 80\%) \sim 0.85$ for 150 nm particles); in addition to potential restructuring, they also stated that other explanations could include larger refractive indices or lower densities for the dry particles as compared to the humidified particles.

A number of laboratory studies focused on inorganic salts have found similar evidence of restructuring, indicating that the mechanism is not limited to organic-containing particles. Aggregated fractal inorganic salt particles shrank after exposure to RHs beyond the RH of formation ($>60\%$ in most cases), and the degree of particle shrinkage was greater for aggregates of larger initial size, as well as larger increases in RH beyond formation RH [Montgomery *et al.*, 2015]. That study suggested that a potential explanation was rooted in surface tension owing to water adsorption within the aggregate structure. At low RH ($<50\%$), restructuring from hydration of $(\text{NH}_4)_2\text{SO}_4$ has been shown to have stronger effects on particle mobility diameter than the adsorption or absorption of water [Mikhailov *et al.*, 2009]. In a study of inorganic salts, observations of the structural rearrangement of NH_4NO_3 , $(\text{NH}_4)_2\text{SO}_4$, NaCl, and NaNO_3 indicated that particle size decreased by up to 10% due to chemical reactions and evaporation upon hydration when exposed to RHs below each salts' respective deliquescence RH [Gysel *et al.*, 2002; Mikhailov *et al.*, 2004]. Another study showed that additive water uptake models overpredict hygroscopic growth for internal mixtures of amino acids and ammonium sulfate [Garland *et al.*, 2007].

Particle coating and photochemical aging affects the ability, degree, and onset of particle restructuring. With regard to coating types, restructuring has been observed with combustion particles coated with H_2SO_4 [Zhang *et al.*, 2008; Pagels *et al.*, 2009], glutaric acid [Xue *et al.*, 2009], dioctyl sebacate and oleic acid [Ghazi and Olfert, 2013], and secondary organic aerosol derived from aromatic precursors [Schnitzler *et al.*, 2014]. Aging soot in the presence of isoprene results in increased mass with decreased particle mobility diameter and increased effective density, as coating material fills in void spaces and causes partial restructuring of fractal soot aggregates [Khalizov *et al.*, 2013]. Photochemical processing of fresh wood smoke was found to physically convert fractal smoke particles into a more spherical shape in addition to concurrent chemical transformations [Giordano *et al.*, 2013; Giordano and Asa-Awuku, 2014].

Particle morphological changes upon hydration, including shrinkage due to restructuring, alter particle light absorption, and scattering characteristics. Shrinkage in the form of restructuring may not necessarily be associated with reduced light scattering. Restructuring by neutralization surface reactions has been suggested to explain reduction in light absorption cross section upon hydration of laboratory generated mixtures of black carbon (BC) and brown carbon (BrC) particles at low RH; however, upon RH increase, continued water uptake by inorganic coatings can lead to absorption enhancement [Chen *et al.*, 2015]. In polluted, humid conditions, it has been observed that hygroscopic particles absorb water and grow in size, enhancing light scattering, but the mass absorption cross section may increase (enhancement between neighboring spherules) or decrease (possibly due to physical shielding effects impacting internal globules of a collapsed agglomerate) [Khalizov *et al.*, 2009; Lee *et al.*, 2012]. Dennis-Smith *et al.* [2012] observed that effective refractive indices of organic aerosol increased during and after evaporation of volatile products and concluded that aging followed by slow restructuring in particle morphology was responsible for this behavior.

The goal of this study is to build on the results of these previous laboratory-based studies by reporting ambient observations of hygroscopic growth (GF and $f(\text{RH})$) < 1 , and consequently $\kappa_e < 0$, from three field projects: Eastern Pacific Emitted Aerosol Cloud Experiment (E-PEACE) in 2011, Studies of Emissions, Atmospheric Composition, Clouds and Climate Coupling by Regional Surveys (SEAC⁴RS) in 2013, and observations from measurement intensive periods at the Tucson Aerosol Characterization Observatory (TACO) between 2014 and 2015. All three field studies included measurements of aerosol hygroscopicity as well as other chemical and meteorological observations. Possible causes for GF and $f(\text{RH})$ below 1 will be discussed and strategies are suggested for probing this phenomenon in greater detail for future studies. The overall objective of the ensuing discussion is to motivate additional examination of archived and future ambient field data sets of aerosol hygroscopic growth to unravel the nature of data points indicative of particle shrinkage after humidification as this affects treatment of aerosol-water interactions in models and remote sensing retrievals of aerosol parameters.

2. Experimental Methods

2.1. Field Observations and Instrumentation

This work uses observations from three field campaigns, with a summary of instrumentation and case study dates provided in Table 1. A more detailed discussion of the experimental approach is provided below.

Table 1. Summary of Field Campaigns, Case Study Dates, Instrumentation, and Measured Parameters for This Study

Campaign	Platform	Full Measurement Period	Case Study	Instrumentation	Measured Parameter
E-PEACE	R/V Point Sur	12–23 July 2011	17 Jul 2011	HTDMA	GF
TACO	Ground-Based	Winter: 30 Jan to 12 Feb 2015; Summer: 27 May to 1 June 2014 12–20 Aug 2014	1 Feb 2015	DASH-SP	GF
SEAC ⁴ SR	NASA DC-8	2 Aug to 13 Sept 2013	19 Aug 2013	DASH-SP LARGE f(RH) AMS PTRMS PALMS HD-SP2	GF f(RH) PM ₁ -Speciated Acetonitrile BB Fraction Black Carbon

2.1.1. E-PEACE Field Campaign

E-PEACE was a multiplatform field study conducted in the coastal zone of California during July–August 2011, investigating aerosol-cloud-precipitation-radiation interactions [Russell *et al.*, 2013]. The project involved the use of the Center for Interdisciplinary Remotely-Piloted Aircraft Studies Twin Otter, based in Marina, CA, and the R/V *Point Sur*, which conducted a 12 day research cruise (12–23 July). Specifics of the campaign and results are detailed elsewhere [Russell *et al.*, 2013; Wonaschütz *et al.*, 2013; Wang *et al.*, 2014; Jung *et al.*, 2015; Modini *et al.*, 2015; Sanchez *et al.*, 2016]. This work utilizes data only from the R/V *Point Sur*, on board of which smoke generators used gasoline and heated paraffin-type oil with low vaporization temperature (150°C) to emit a plume of thick condensed smoke and organic vapor into the marine boundary layer. The smoke was measured from R/V *Point Sur* itself with an extensive payload of instruments [Russell *et al.*, 2013].

Of most relevance from the R/V *Point Sur* instrument payload was a HTDMA, which measured hygroscopic growth using two DMAs, with one dry ($RH_{dry} < 8\%$) and one humidified at varying RH settings (40, 70, 85, and 92%). The HTDMA uncertainty in GF is ± 0.03 [Lopez-Yglesias *et al.*, 2014]. Dry particle diameters ($D_{p,dry}$) selected were 30, 75, 150, and 300 nm. To compare to high RH set points in similar studies, we focus on set points of RH = 85 and 92% and dry diameters of 150 and 300 nm. Smoke emitted from the ship and then resampled by the ship on 17 July 2011 constitutes a key case study. Plume tracking, meteorological conditions, and results from other instruments on board R/V *Point Sur* related to the smoke sampling can be found in Wonaschütz *et al.* [2013]. As noted in the latter study, differences used to distinguish between smoke and nonsmoke periods included particle number concentration (nonsmoke periods: $< 1000 \text{ cm}^{-3}$; smoke periods: $> 1000 \text{ cm}^{-3}$) and aerosol composition (smoke periods: organic mass fraction $\geq 97\%$ based on submicrometer measurements of nonrefractory aerosol species and nonsmoke periods: organic mass fraction $\sim 40\text{--}60\%$).

2.1.2. TACO Measurement Intensives

The Tucson Aerosol Characterization Observatory (TACO) is a rooftop laboratory on the University of Arizona campus in central Tucson (30 m above ground level, 720 m above sea level; 32.2299°N, 110.9538°W), which has a metropolitan population of approximately one million [U.S. Census Bureau, 2011]. The observatory has been collecting long-term data relevant to aerosol particle properties and meteorology since 2009. Observations at TACO from various instruments in addition to DASH-SP such as a Particle-Into-Liquid Sampler (Brechtel Manufacturing Inc.), cloud condensation nuclei counter (CCNC, DMT Inc.), a semicontinuous OC/EC analyzer (Sunset Laboratory Inc.), Micro-Orifice Uniform Deposit Impactors (MSP Corporation), and single-stage filter samplers, are summarized elsewhere [Youn *et al.*, 2013; Crosbie *et al.*, 2015; Sorooshian *et al.*, 2015; Youn *et al.*, 2015].

During TACO intensives, the DASH-SP measured size-resolved GFs at humidified RH values typically between 50 and 95% with dry channel measurements below 20% RH, and with $D_{p,dry}$ between 180 and 300 nm. The DASH-SP RH was controlled within 1.5% of the RH set point, and the GF uncertainty was less than 3% [Shingler *et al.*, 2016]. The instrument data from TACO relevant to the current study are from the DASH-SP during summer intensive periods (27 May to 1 June 2014 and 12–20 August 2014) and a winter intensive period (30 January to 12 February 2015). Scan times were held constant at 80 s during the winter intensive and 90 s during the summer intensive to allow for a consistent sampling schedule between the DASH-SP and other instruments.

The DASH-SP instrument is composed of a DMA linked to a humidification and optical sizing system. The DMA is used to separate dried particles into a monodisperse sample flow based on electrical mobility size. The monodisperse flow is then separated into two flows, both sent to individual optical particle counters (OPCs) measuring optical light scattering intensity in the form of electrical pulse heights. One OPC directly measures scattering of the dried monodisperse particles in order to determine the real portion of the dry effective refractive index, RI_{dry} ($\lambda = 532$ nm), while the other measures scattering of particles that have passed through a diffusion-based humidifier. The combination of the dry particle size, RI_{dry} , and humidified scattering intensity allows the wet particle diameter to be determined. Instrument operating details, data processing procedures, and examples of its field deployment are presented elsewhere [Sorooshian *et al.*, 2008a; Sorooshian *et al.*, 2008b; Hersey *et al.*, 2009; Hersey *et al.*, 2011; Hersey *et al.*, 2013; Shingler *et al.*, 2016].

2.1.3. SEAC⁴RS Field Campaign

Based out of Houston, TX, during August–September 2013, SEAC⁴RS incorporated three research aircraft to investigate numerous topics including (i) redistribution of emissions throughout the troposphere from deep convection, (ii) evolution of gases and aerosols in convective outflow and their implications for atmospheric chemistry, and (iii) how anthropogenic pollution and biomass burning emissions are affected by meteorology and cloud processing. Another focus was to validate/calibrate instrumentation as a test bed for future applications. Details of the SEAC⁴RS project and specifics on measurements pertaining to this work can be found elsewhere [Toon *et al.*, 2016], and all data are publicly available from the NASA Langley Research Center's Atmospheric Science Data Center [Atmospheric Science Data Center, 2015].

This work focuses on in situ measurements from the NASA DC-8, utilizing all research flights from SEAC⁴RS with focus on three flights that targeted biomass burning sampling: 6 August, 19 August, and 27 August. Sample air fed to the hygroscopicity instruments (DASH-SP and nephelometers) on the DC-8 is brought into the aircraft through an isokinetically controlled inlet, tested in a previous flight experiment, and shown to efficiently collect and transmit particles smaller than 4 μ m diameter [McNaughton *et al.*, 2007]. Sample air is actively dried using a nafion dryer (Perma-Pure FC-125-240-10PP), which efficiently passes accumulation-mode aerosol. The DASH-SP on board the DC-8 measured size-resolved hygroscopic GFs of ambient aerosol particles at humidified RH values typically between 70 and 95% with dry channel measurements below 15% RH, and $D_{p,dry}$ between 175 and 350 nm [Shingler *et al.*, 2016]. Polystyrene latex spheres (PSLs) were used during flight to calibrate instrument uncertainty for the aerosol-sampling package aboard the DC-8, details of which for the DASH-SP can be found in Shingler *et al.* [2016]. Similar to TACO conditions, the DASH-SP RH was controlled to within 1.5% of RH set point, and GF uncertainty was less than 3% [Shingler *et al.*, 2016]. DASH-SP scan sampling duration ranged from 1 s to 182 s with an average of 15.5 s, sampling an average of 248 ± 302 and 221 ± 340 particles per scan in the dry and humidified channels, respectively.

$f(RH)$ data for bulk aerosol are obtained from the Langley Aerosol Research Group Experiment (LARGE) instrument package, specifically the tandem humidified nephelometers (TSI Inc, St. Paul, MN, USA; Model 3563) [Ziemba *et al.*, 2013] at dry (RH 20%) and humidified (RH 80%) scattering channel settings, and with a reported uncertainty in $f(RH)$ of ± 0.05 . $f(RH)$ is calculated as the ratio of humidified scattering coefficient to dry scattering coefficient at 550 nm. Nephelometer data were recorded and archived every second at three wavelengths (450, 550, and 700 nm). In terms of operation, part of the air sampled through the isokinetically controlled inlet is fed to one nephelometer that receives no further sample treatment, while the rest of the air is humidified in a second nephelometer in the following manner. Dry sample air flow is split into a sheath flow (5 L min^{-1}) and sample flow (22 L min^{-1}). The sheath flow is humidified using one nafion humidifier (Perma-Pure FC-125-240-5PP) with counterflowing heated water (controlled to approximately 45°C for SEAC⁴RS). This saturated flow is subsequently routed through the sheath of a second sample humidifier, thus increasing the RH in the 22 L min^{-1} sample flow. The sample RH is controlled by cycling the sample sheath air between saturated and dry air to achieve a set point (e.g., 80% \pm 4%). This is accomplished using a PID (proportional-integral-derivative) process controller (Edwards, model 501C) and electrically actuated three-way valve. The RH measured at the nephelometer inlet (control-RH) is measured with an insulated, external sensor (Vaisala, model HMP60). An additional sensor inside the instrument is used for the $f(RH)$ calculation. Differences between the instrument-RH and the control-RH were less than 5% (an average deviation of 3.3%) during SEAC⁴RS. Because of its active feedback, this system automatically adjusts for variable RH of input air (which varied typically between 10 and 30%),

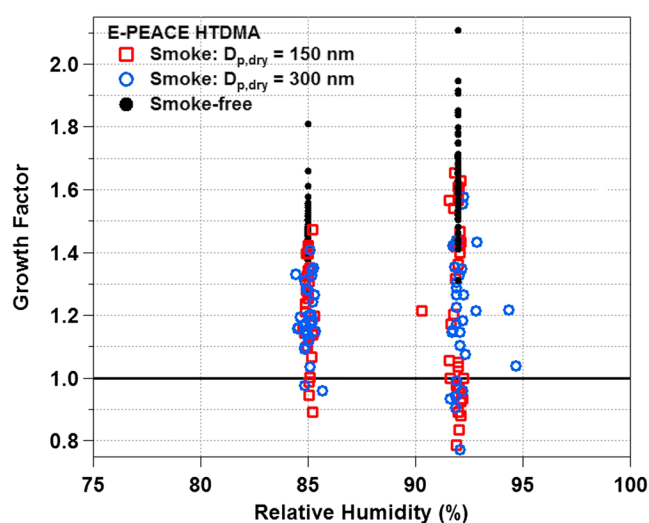


Figure 1. Growth factor as a function of HTDMA RH (85% and 92%) during E-PEACE for $D_{p,dry}$ values of 150 nm and 300 nm for smoke sampling from 17 July 2011. Data are shown for all nonsmoke sampling days with 150 and 300 nm $D_{p,dry}$ grouped together as those two sizes showed no significant difference.

ambient pressure, and cabin temperature to maintain a constant RH in the nephelometer. Nephelometer data are manually synchronized to compensate for additional lag time incurred in the humidified sample line. Transport efficiency was determined for the sample humidifier in the laboratory prior to SEAC4RS deployment showing 100% transmission up to 0.6 μm diameter that is reduced to 78% transmission at 1 μm , indicative of efficient sampling of the various aerosol types encountered such as biomass burning aerosol.

Identical angular truncation error corrections detailed in *Anderson and Ogren* [1998] were applied to each nephelometer. Both nephelometers were calibrated with filtered air and pure CO_2 before, during, and after SEAC4RS. In-flight calibration

using PSLs of different sizes (i.e., 102, 200, 269, 600, and 1000 nm) confirmed consistent instrument response on a flight-by-flight basis (i.e., $f(\text{RH})=1$). Independent verification of the LARGE extinction/hygroscopicity measurement has been demonstrated for urban aerosol by comparison with collocated airborne High Spectral Resolution Lidar [Ziemba *et al.*, 2013].

Other DC-8 data used in this work include the following: (i) acetonitrile from the Proton-Transfer-Reaction Mass Spectrometer (PTRMS) [de Gouw and Warneke, 2007]; (ii) black carbon (BC) from the Humidified-Dual Single-Particle Soot Photometer, with diameter range $\sim 90\text{--}550$ nm assuming 1.8 g cm^{-3} density, which is typically $\sim 90\%$ of accumulation-mode mass (HD-SP2) [Schwarz *et al.*, 2015]; (iii) submicrometer aerosol (PM_{10}) chemical composition from the High Resolution Aerosol Mass Spectrometer (HR-AMS) [DeCarlo *et al.*, 2006; Canagaratna *et al.*, 2007]; (iv) biomass burning (BB) number fraction from the Particle Analysis by Laser Mass Spectrometry, with size range 200–3000 nm (PALMS) [Lee *et al.*, 2002]; and (v) size distribution data from the Laser Aerosol Spectrometer (LAS; D_p between 0.1 and 6.3 μm) and Ultra-High Sensitivity Aerosol Spectrometer (UHSAS; D_p between 63 and 891 nm), which are both a part of LARGE. Data from three of these instruments with similar size ranges were used to quantify effective particle density under the assumption of spherical particles. Density is calculated as the mass concentration sum of HR-AMS species (organic, sulfate, nitrate, ammonium, and chloride) and HD-SP2 BC, divided by integrated volume from the UHSAS. For the various instruments described from SEAC4RS, data contamination during cloud penetrations (i.e., affected by droplet shattering on the inlet tip) was identified visually and removed.

3. Results

3.1. Hygroscopic Growth Factor and $f(\text{RH})$ Observations

Ship-based HTDMA measurements of GF at RHs of 85% and 92% during E-PEACE are summarized in Figure 1. GFs are clearly suppressed in smoke-influenced samples as compared to background aerosol sampled outside of the ship-generated smoke plume. GFs below 1.25 are only observed in smoke-influenced samples. Additionally, numerous observations of $\text{GF} < 1$ are reported during smoke sampling, regardless of $D_{p,dry}$ (150 and 300 nm particles are shown for simplicity). For smoke data at $\text{RH} = 85\%$, $\sim 7\%$ (2 of 28) and $\sim 10\%$ (3 of 29) of points exhibited $\text{GF} < 1$ at 300 nm and 150 nm, respectively, while at $\text{RH} = 92\%$, $\sim 19\%$ (6 of 32) and 31% (10 of 32) of points exhibited $\text{GF} < 1$ at 300 nm and 150 nm, respectively. Minimum values of GF during smoke sampling included 0.89 and 0.77 at RHs of 85 and 92%, respectively.

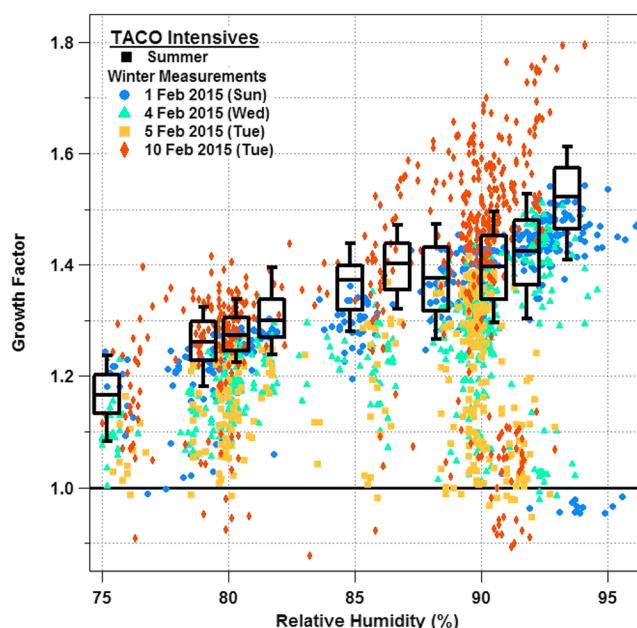


Figure 2. Growth factor as a function of DASH-SP RH for $D_{p,dry}$ values of 190–300 nm. Data are shown separately for the 4 days when $GF < 1$ values were observed during the TACO winter intensive period, with box and whiskers for the entire summer intensive measurement period. Whiskers represent 10–90% of data, boxes represent 25–75% of data, and median is a horizontal bar inside boxes.

Ground-based measurements of GF for $D_{p,dry}$ of 190–300 nm during TACO intensives (Figure 2) indicate that higher values are observed during summer periods (above 1.15 at $RH > 80\%$) with a greater number of days showing suppressed GFs, including values below 1, during winter periods. Data from only those 4 days during the winter intensive with $GF < 1$ are shown, with 76% of the $GF < 1$ observations being between the hours of 04:00 and 08:00 (local time). During those 4 days, 3% (53 of 1777) of the data points exhibited $GF < 1$, with a minimum value of 0.88. The frequency of occurrence of $GF < 1$ was greater for $RH > 90\%$ (5.5%; 36 of 658 points) as compared to $RH < 90\%$ (1.5%; 17 of 1119 points). Winter in the Tucson metropolitan area is characterized by enhanced residential burning for heat leading to increased $PM_{2.5}$ levels nearing exceedance of National Ambient Air Quality Standards [Kramer *et al.*, 2015]. As the area is

surrounded by mountains with strong boundary layer inversions during cold nights, residential burning emissions are trapped in a shallow layer and often are not ventilated in periods of prolonged cooler temperatures [Crosbie *et al.*, 2015], leading to the highest year-round $PM_{2.5}$ mass concentrations of species linked to biomass burning, which include elemental carbon, organic carbon, and water-soluble organic carbon [Youn *et al.*, 2013]. While it cannot be proven unambiguously that GFs less than 1 in Tucson are due to biomass burning, certainly, the overlap in time of burning during periods with these data points supports the case for a potential link.

Hygroscopicity data from SEAC⁴RS for $D_{p,dry}$ of 180–400 nm indicate that 1% (31 of 2429) of data points during the three flights with $GF < 1$ values exhibited such values, with a minimum value of 0.95 (Figure 3). Similar to E-PEACE and TACO, a difference in trends between biomass burning and nonsmoke samples is observed, with $GF < 1$ points observed only during the former periods. Shingler *et al.* [2016] showed that wildfire emissions during SEAC⁴RS coincide with suppressed GF, including data values below 1. They classified air masses as being impacted by wildfire biomass burning when acetonitrile exceeded 250 pptv. During all wildfire biomass burning sampling, ~2% of biomass burning sampling resulted in $GFs < 1$, while ~75% of $f(RH)$ values were less than 1. A number of the $GF < 1$ points in Figure 3 are outside of the measurement uncertainty (<3%) and correspond to $f(RH) < 1$ values. For flights on 6 and 19 August, ~95% of $f(RH) < 1$ points are in biomass burning air masses, and on 27 August only ~50% of $f(RH) < 1$ samples are associated with biomass burning, with the remainder of $f(RH) < 1$ observations in mixed air masses in the boundary layer or in the free troposphere.

From the three presented field studies, biomass burning (SEAC⁴RS), wintertime aerosol with effects from likely residential wood burning (TACO), and paraffin smoke emissions (E-PEACE) coincide with suppressed GF observations and hygroscopicity (i.e., GF and/or $f(RH)$) less than 1 compared to periods with less influence from smoke and carbonaceous-rich particles. It is important to stress that GF and $f(RH)$ values above 1 in these data sets do not preclude the possibility that subsequently discussed mechanisms are still at work that are thought to lead to sub-1 values (e.g., restructuring), but it becomes much more challenging to untangle such effects from concurrent water uptake for such data points.

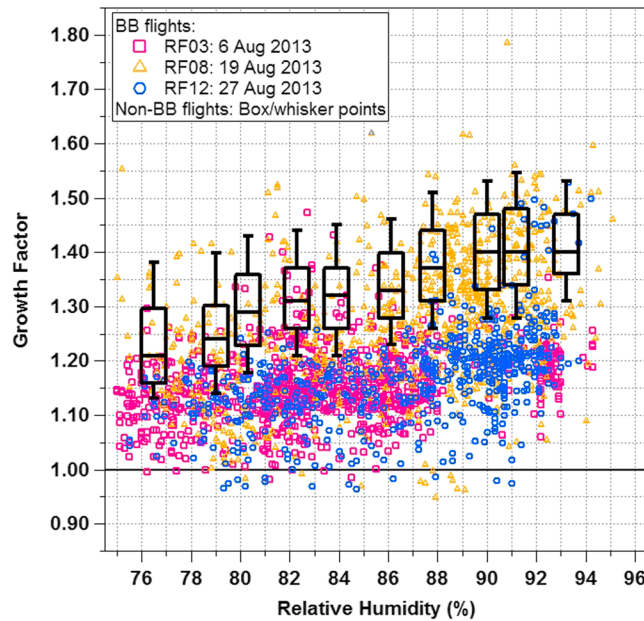


Figure 3. Growth factor as a function of DASH-SP relative humidity for all SEAC⁴RS flights, for $D_{p,dry}$ values of 180–400 nm. Data are shown separately for all nonbiomass burning flights (black box and whisker points) and three biomass burning-focused flights (colored dots) coinciding with all of the $GF < 1$ data.

3.2. Case Study: Aged Smoke Sampling

For a more in-depth investigation of GF and $f(RH)$ values below 1, a case study is highlighted from the SEAC⁴RS flight on 19 August 2013. A flight from this campaign is chosen for a case study as it had a more complete suite of instruments than the other campaigns and the measurements cover biomass burning plumes across a wider plume age range. Note that while this flight’s observations indicate $f(RH) < 1$ was always measured when $GF < 1$, GF is not always below 1 when $f(RH) < 1$; hence, these measurements are not always harmonious, and the lack of consistency between κ_e (or $GF(RH=80\%)$) and $f(RH=80\%)$ values is believed to be due to size-dependent composition, as was also suggested by Shingler *et al.* [2016]. During this flight, the DC-8

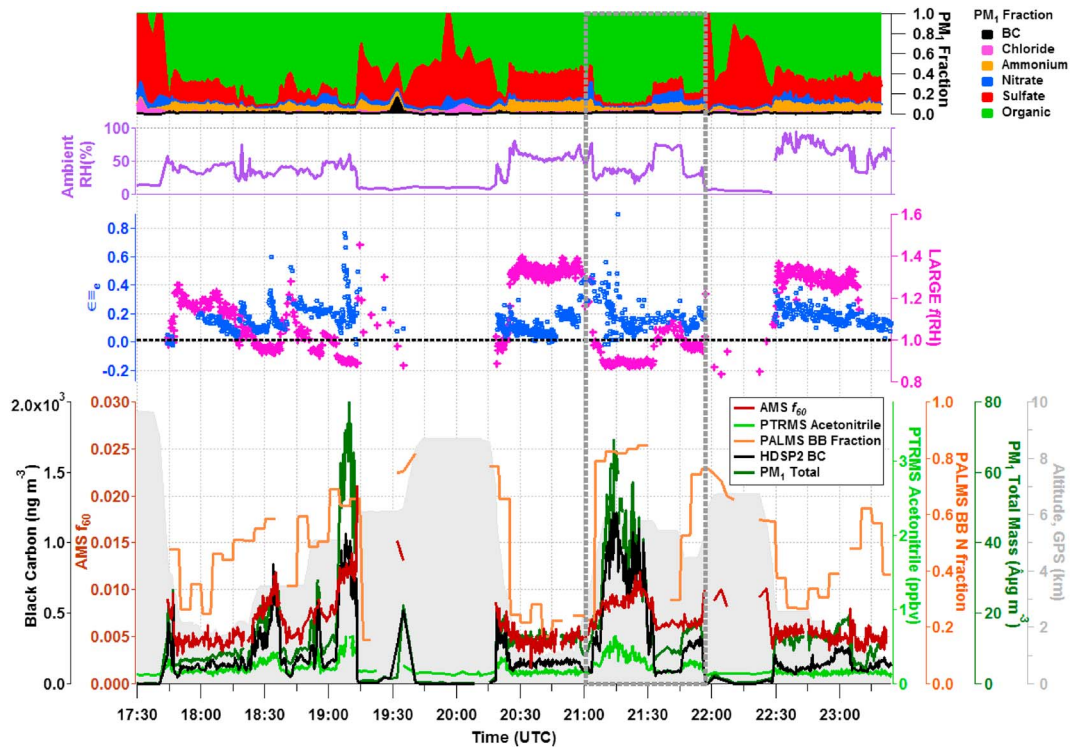


Figure 4. Time series of chemical composition, ambient relative humidity, hygroscopicity measurements (κ_e derived from DASH-SP GF values for $D_{p,dry}$ values of 180–400 nm, and $f(RH)$), aircraft altitude, and biomass burning tracers for the SEAC⁴RS 19 August 2013 flight. This flight targeted aged wildfire smoke, with 21:00–22:00 highlighted (dashed gray box) since this period is referred to in Figure 10.

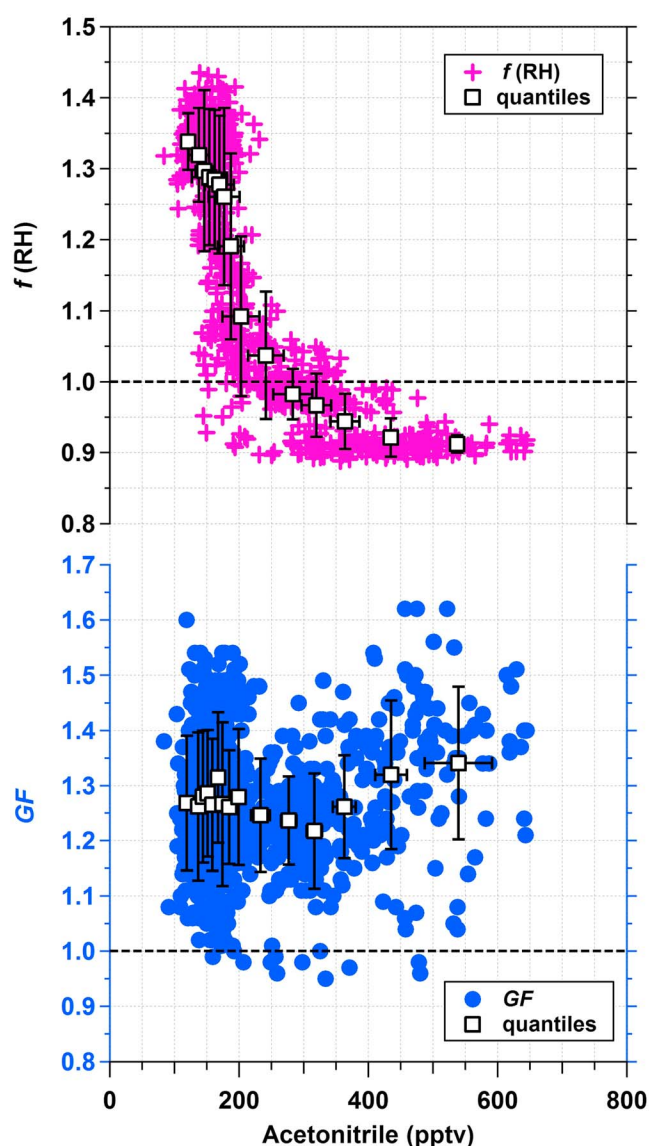


Figure 5. LARGE $f(\text{RH})$ and DASH-SP GF as a function of acetonitrile, a biomass burning marker, for the SEAC⁴RS 19 August 2013 flight. The GF data are for a $D_{p,\text{dry}}$ range of 160–360 nm and RHs between 75 and 95%.

discrepancy is that $f(\text{RH})$ is a bulk measurement unlike the DASH-SP. Shingler *et al.* [2016] have shown with the SEAC⁴RS data set that the only way the DASH-SP GF (and thus κ_e) and LARGE $f(\text{RH})$ data can be reconciled is if GF exhibits variability as a function of dry size.

The relationship between hygroscopic growth and biomass burning indicators is further explored in Figure 5 where it is shown that acetonitrile and $f(\text{RH})$ have an inverse relationship asymptotically approaching $f(\text{RH}) \sim 0.9$ at the highest acetonitrile concentrations (550–650 pptv). $f(\text{RH})$ values were always below 1 when acetonitrile levels exceeded 380 pptv. The relationship between GF and acetonitrile is much less clear, most likely due to the size-resolved nature of DASH-SP measurements.

In contrast to observed sub-1 values for $f(\text{RH})$ and GF, the HD-SP2 data show no reduction in scattering from BC-containing particles upon humidification in biomass burning plumes during SEAC⁴RS [Perring *et al.*, 2016]. This indicates that any widespread particle restructuring is not happening for the subpopulation of BC-containing aerosol particles as has been observed in laboratory studies of fresh smoke [e.g., Onischuk *et al.*, 2003;

probed an aged fire plume over Nebraska and Wyoming, originating from Idaho and Wyoming fires as determined from the emission inversion method [Saide *et al.*, 2015].

Figure 4 presents a time series of chemical composition, biomass burning markers, aircraft altitude, ambient RH, and hygroscopicity measurements. The biomass burning markers utilized in this study are as follows: (i) gas-phase acetonitrile, indicative of biomass burning emissions at elevated concentrations (>250 pptv) [Shingler *et al.*, 2016]; (ii) AMS f_{60} , which is the fraction of organic aerosol at m/z 60 (dominated by the contribution of $\text{C}_2\text{H}_4\text{O}_2^+$, a levoglucosan-like fragment) [Cubison *et al.*, 2011] to total organic aerosol; (iii) BC; and (iv) PALMS biomass burning (BB) fraction (i.e., number fraction in $\text{PM}_{2.5}$ containing biomass burning material) [Froyd *et al.*, 2010].

The periods of lowest $f(\text{RH})$ between 21:00 and 21:30 correspond to enhanced levels of all four of the aforementioned biomass burning tracers. Although the mass fraction of BC relative to total PM_1 (MF_{BC}) remains steady in and out of biomass burning plumes (~ 1 –2%), organic mass fraction was enhanced in biomass burning plumes, which explains the reduction in $f(\text{RH})$ during this period. Values of κ_e derived from DASH-SP data are also lowest during this period; however, only a few points exhibited values of $\kappa_e < 0$. A plausible explanation for this discrepancy

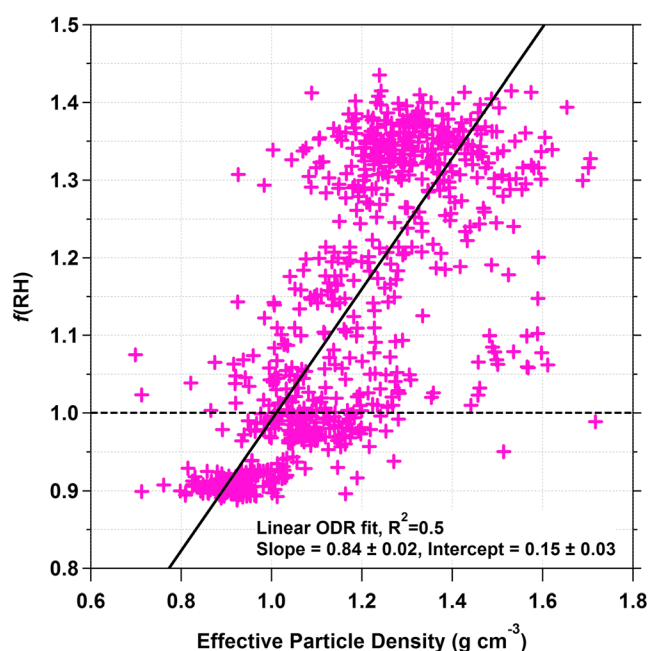


Figure 6. LARGE $f(\text{RH})$ as a function of optically derived effective particle density for the SEAC⁴RS 19 August 2013 flight.

particle restructuring potential. Effective particle density is calculated from UHSAS size distributions ($\text{RI}_{\text{dry}} = 1.52$) and chemical composition data from the HR-AMS and HD-SP2. Figure 6 illustrates the relationship between optically derived effective particle density and $f(\text{RH})$, which both are representative of bulk aerosol unlike the size-resolved GF measurements from the DASH-SP. $f(\text{RH})$ increases as a function of effective particle density. A linear orthogonal distance regression trend line is fit to the $f(\text{RH})$ -density scatterplot, resulting in slope of $0.84 \text{ cm}^3 \text{ g}^{-1}$, and R^2 of 0.5 ($n = 747$). While this analysis cannot provide direct proof, especially since particle density also depends on composition, the effective density correlation with $f(\text{RH})$ is at least supportive of the possibility that there is greater particle restructuring potential in periods with $f(\text{RH}) < 1$.

4. Discussion

Sections 4.1 and 4.2 focus on reasons as to why hygroscopic growth below 1 may be observed in the various data sets presented in this work. One mechanism is already discussed in section 1, that the current data set cannot provide direct evidence for, but is a potential explanation for at least a subset of the data, is particle restructuring. It is possible that restructuring can occur concurrently with any combination of the other reasons discussed below. Section 4.3 demonstrates how a revised DASH-SP data processing strategy can handle cases of externally mixed aerosol in order to identify more cases of $\text{GF} < 1$ than the previously used data processing method allowed. While we cannot unambiguously prove which combination of factors is responsible for specific data points with GF and $f(\text{RH}) < 1$, the discussion below is intended to motivate future work to improve understanding of why such data points exist.

4.1. Refractive Index Sensitivity

Since the DASH-SP data processing algorithm relies on the measurement of the real part of dry particle effective RI_{dry} , it is possible that a change in effective RI_{dry} , due to either physicochemical modification in the DASH-SP after dry sizing or incorrect identification of effective RI_{dry} , could result in an apparent change in wet size. To probe this possibility, we analyzed GF sensitivity to effective RI_{dry} perturbations. Results for a representative humidified channel RH (85%) and OPC electrical pulse height (PH_{wet} : 30,000 in Figures 7a and 7b) are presented here, although a large range of possible conditions were examined. Note that electrical pulse heights and counts in each pulse height bin are related to diameter and number concentration,

Khalizov *et al.*, 2013]. One plausible reason is that in atmospheric measurements of biomass burning aerosol there is virtually no access to truly “fresh” emissions, as dilution, transport, and chemical processing occur after emission. HD-SP2 measurements indicate that the BC-containing particles in the plumes were thickly coated unlike the highly aggregated fractals observed in laboratory experiments, so it is possible that the BC in these particles had already “collapsed” prior to our measurements, due to condensation of coatings.

As wetting of chain-like or aggregated particles can lead to a more compact particle with higher density [Weingartner *et al.*, 1995; Jimenez *et al.*, 2003; Onischuk *et al.*, 2003; Lewis *et al.*, 2009], differences in effective particle density are used here as a qualitative marker for par-

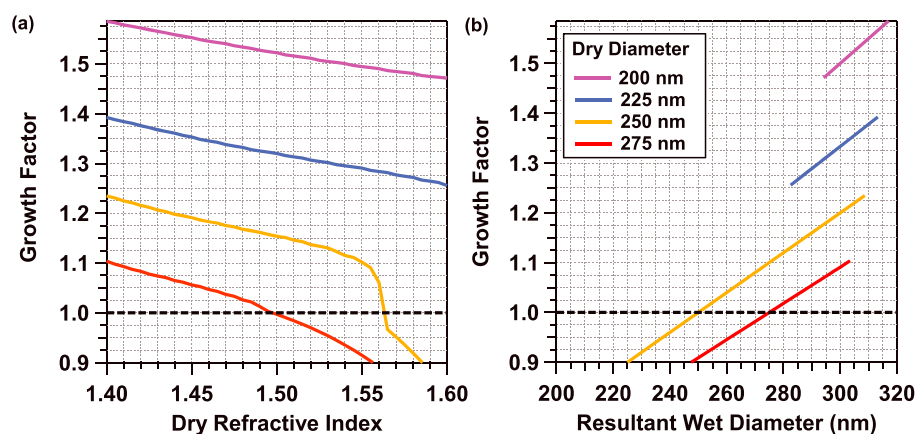


Figure 7. Visualization of the sensitivity of DASH-SP GFs to perturbations in effective $R_{l,dry}$ that could arise during humidification for PH_{wet} of 30,000 and RH of 85%. $R_{l,dry}$ is shown as a function of both GF and resultant wet diameter for different $D_{p,dry}$ values. A GF value of 1 is marked for reference (black dotted line).

respectively. For a given $D_{p,dry}$, RH, and fixed PH_{wet} , the impact of effective $R_{l,dry}$ perturbations on GF and “resultant” wet diameter was calculated assuming that humidified physical size does not change (i.e., the effect of effective $R_{l,dry}$ on GF is isolated). For a fixed $D_{p,dry}$ and wet physical size ($D_{p,wet}$), a shift in effective $R_{l,dry}$ produces a profound effect. A 275 nm dry particle could have a GF ranging from 0.9 to 1.1 over an effective $R_{l,dry}$ range of 1.4–1.56 (Figure 7a). This translates to a resultant wet diameter range from 248 to 302 nm (Figure 7b).

It is also important to consider that particles that have an imaginary component of the refractive index will be vulnerable to effects on the OPC scattering signal, and thus values of the derived effective $R_{l,dry}$, in the DASH-SP [Shingler *et al.*, 2016]. As the BC content of the ambient particles, especially during biomass burning periods in SEAC⁴RS, was usually quite small (submicrometer aerosol mass fraction < 2%), it is presumed that the impact of absorbing components on the DASH-SP effective $R_{l,dry}$ measurements was insignificant. However, future work will aim to address this issue with targeted laboratory experiments.

4.2. Evaporation and Phase Change

If a particle experiences evaporative losses in the DASH-SP after selection of a dry size up to the point of the humidified OPC measurement, $GF < 1$ could result in particles that originally were hydrophobic with GFs near and just above unity. As there is insignificant dilution or temperature change in the $f(RH)$ measurement technique, evaporative losses are less of an issue for $f(RH)$ measurements as compared to DASH-SP measurements of GF. Since $f(RH)$ data points represent the majority of hygroscopicity observations less than 1 during SEAC⁴RS (Figures 4 and 5), it is unlikely that evaporative losses are the dominant contributing mechanism in at least that field campaign. However, an examination of the magnitude of such losses is more relevant to the TACO and E-PEACE measurements with the DASH-SP and HTDMA, respectively. Here we report on thermokinetic modeling results of evaporative losses in the DASH-SP instrument, as introduced by Shingler *et al.* [2016] with model simulation details from that study repeated in Text S1 (supporting information) [Shingler *et al.*, 2016; Shiraiwa *et al.*, 2012; Zuend *et al.*, 2008, 2011]. In contrast to the latter study, we examine losses only after dry particle sizing rather than from the instrument inlet.

When considering a range of conditions associated with ambient temperatures (250, 295, and 310 K) for particles with plausible relative amounts of inorganics and organics (5% ammonium nitrate, 25% ammonium sulfate, 50% low volatility organic compounds (LVOCs), and 20% semivolatile organic compounds (SVOCs)), evaporative losses relative to the initial sampled dry particle mass concentrations were appreciable for liquid-phase particles. More specifically, losses associated with ammonium nitrate ranged between 13.1 and 14.3% at the three ambient temperatures examined (ambient and DASH-SP sampling RH fixed at 60% and 85%, respectively). Losses of organics range from near zero for low volatility compounds such as docosanoic acid (~0.01%), to 5.6–11.2% for more volatile species such as chrysene. Losses of SVOCs and

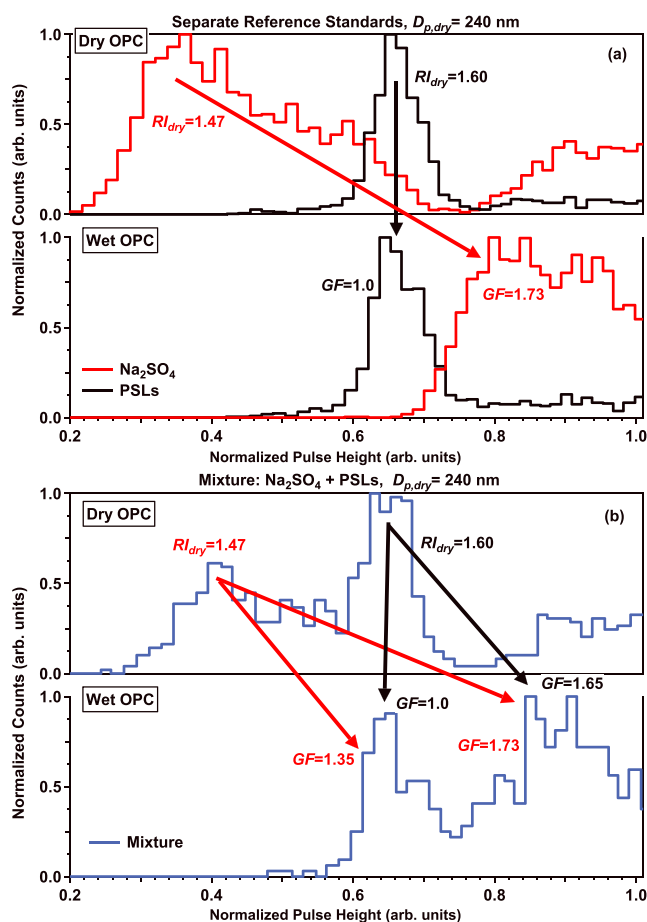


Figure 8. DASH-SP laboratory characterization results ($D_{p,dry} = 240$ nm, 80% RH) when sampling (a) separate calibration standards (Na_2SO_4 and PSLs) and (b) the mixture of the two standards. Figure 8b shows that if the composition of the aerosol was unknown that four different GF values would be possible.

homogeneous mixture of aerosol particles. Focused laboratory experiments were conducted, and improvements to the DASH-SP data processing algorithm were made to demonstrate how identification of external mixtures can yield more instances of $\text{GF} < 1$.

To test the DASH-SP's capability to identify the presence of externally mixed aerosol, calibration standard solutions of Na_2SO_4 , PSLs, and a mixture of the two were atomized and fed to the instrument, which sampled at a $D_{p,dry}$ of 240 nm with $\text{RH} = 80\%$ (Figure 8). These two species were chosen for their discretely different RI_{dry} and GF properties. The RI_{dry} values, measured in the dry OPC channel, of the two number concentration modes correctly match the values of the individual standards, where RI_{dry} is 1.47 for Na_2SO_4 and 1.60 for PSLs. While individual standards produce one clear number concentration mode, and thus one GF, according to the properties of each specific standard (Figure 8a), a mixture of the two species results in more ambiguity (Figure 8b). As this was a controlled laboratory experiment, it is known with certainty how the two modes in each distribution of Figure 8b match up. However, if this were a field measurement, the unknown composition of particles resulting in two distinct effective RI_{dry} values makes it challenging to assign the two humidified peaks to the two effective RI_{dry} values. This results in four potential GFs from the mixture sample scan (Figure 8b). In the following discussion (Figures 9 and 10), we define an external mixture as being when two distinct effective RI_{dry} values are observed at a single $D_{p,dry}$.

DASH-SP scans were selected that represent cases of externally mixed aerosol from SEAC⁴RS (Figure 9a) and TACO (Figure 9b). The scans selected are representative of smoke sampling periods, with the caveat that

ammonium nitrate are negligible ($\leq 0.01\%$) when considering semisolid particles. These reported evaporative losses for liquid-phase particles in the instrument would reduce a GF of 1.15, 1.17, and 1.17 (without losses) to 1.11, 1.15, and 1.15 (with losses) for ambient temperatures of 250, 295, and 310 K, respectively. As the modeled semivolatile composition within the particle phase is representative of most ambient samples, it can be qualitatively assumed that a reported GF just below unity could be higher without evaporative losses within the sampling inlet and DASH-SP system. Paraffin smoke sampled during E-PEACE (yielding $\text{GF} < 1$) was 99% organic on a mass basis and likely much more volatile than typical ambient particles; therefore, evaporative losses leading to $\text{GF} < 1$ could be possible in the HTDMA as also suggested by Mochida and Kawamura [2004].

4.3. External Mixtures

Atmospheric aerosol particles are often assumed to be internally mixed due to atmospheric processing. An external mixture is a heterogeneous mixture of aerosol particle populations, where each particle may have unique composition, whereas an internal mixture is a chemically

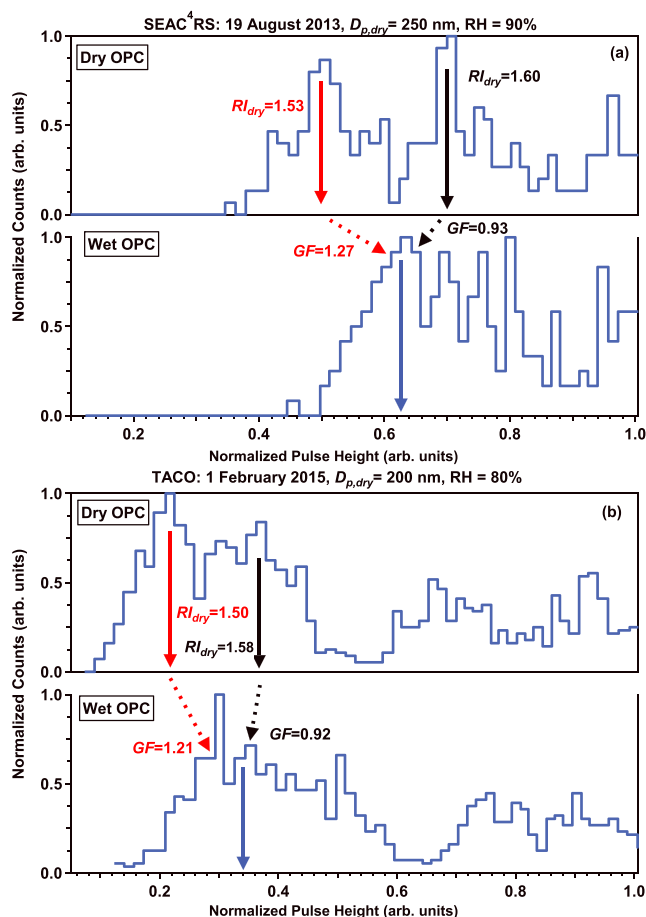


Figure 9. Examples of the DASH-SP detecting externally mixed aerosol, and thus multiple GFs, during (a) the SEAC⁴RS campaign and (b) wintertime intensive measurement period at TACO.

TACO data do not reflect a fresh smoke plume but rather a wintertime urban plume with likely smoke influence during a night with low ambient temperatures ($\sim 7^{\circ}\text{C}$). The modes in the humidified size distributions are less defined for these two cases, and there is uncertainty about how to match each effective RI_{dry} with an associated humidified channel mode. Depending on which of the effective RI_{dry} values is associated with the weighted mean of the humidified OPC distribution, two GFs are possible, and in these cases, the higher effective RI_{dry} results in a GF value below 1. This analysis suggests that instances of $\text{GF} < 1$ could generally be underreported with current postprocessing algorithms (as used with DASH-SP measurements up to this point) that can only result in one GF value per scan. However, if this approach is applied widely, it could also lead to false reports of GF values less than 1 since peaks could be “hiding” in the humidified distribution, which may lead to mismatched peaks between dry and humidified scans.

The reported GFs for DASH-SP scans in Figures 9a and 9b are instead 1.26 and 1.16, respectively, using the weighted mean approach of Shingler *et al.* [2016], which only permits one reported GF per scan.

To further investigate external mixtures during the case study flight on 19 August 2013 during SEAC⁴RS, Figure 10 shows a time series of dry and humidified OPC scans from 21:00 to 22:00 with κ_e and $f(\text{RH})$. Changes in selected $D_{p,\text{dry}}$ are reflected in location of dry OPC distributions. During the period in Figure 10, the DC-8 spent time in and out of biomass burning plumes. This distinctive signature of being either in or out of the plume is evident with $f(\text{RH})$ values below 1 in the plume. Evidence of prolonged periods of the DASH-SP sampling external mixtures, as seen by bimodal profiles of electrical pulse heights, is correlated with periods of $f(\text{RH}) < 1$. The effect of two populations of aerosol at one $D_{p,\text{dry}}$ supports the claim that the DC-8 sampled an externally mixed aerosol population during biomass burning plumes on 19 August 2013.

It is worth noting that roughly 50% of pulse height observations in DASH-SP raw data during periods of externally mixed aerosol are at the higher effective RI_{dry} value, which has a similar effective RI_{dry} to BC or PSLs ($\text{RI} \geq 1.6$). Typical organic aerosol has an effective RI of 1.55, and elemental carbon has an RI of 1.8 [Malm *et al.*, 2005]. It has been suggested that amorphous carbon spheres or “tar balls” with higher RI than individual organic molecules could be responsible for the second higher effective RI peak, particularly in the $D_{p,\text{dry}}$ size range of interest in this work (175–350 nm) [Hand *et al.*, 2005]. A more recent study of tar balls found them to have an average RI of 1.84–0.21i at 550 nm [Hoffer *et al.*, 2016]. These tar balls are thought to consist of organic polymer material and are mostly insoluble in water [Posfai *et al.*, 2004], unchanged by moderate RH or cloud processing. However, Hand *et al.* [2005] suggested that at $\text{RH} > 80\%$, scanning electron

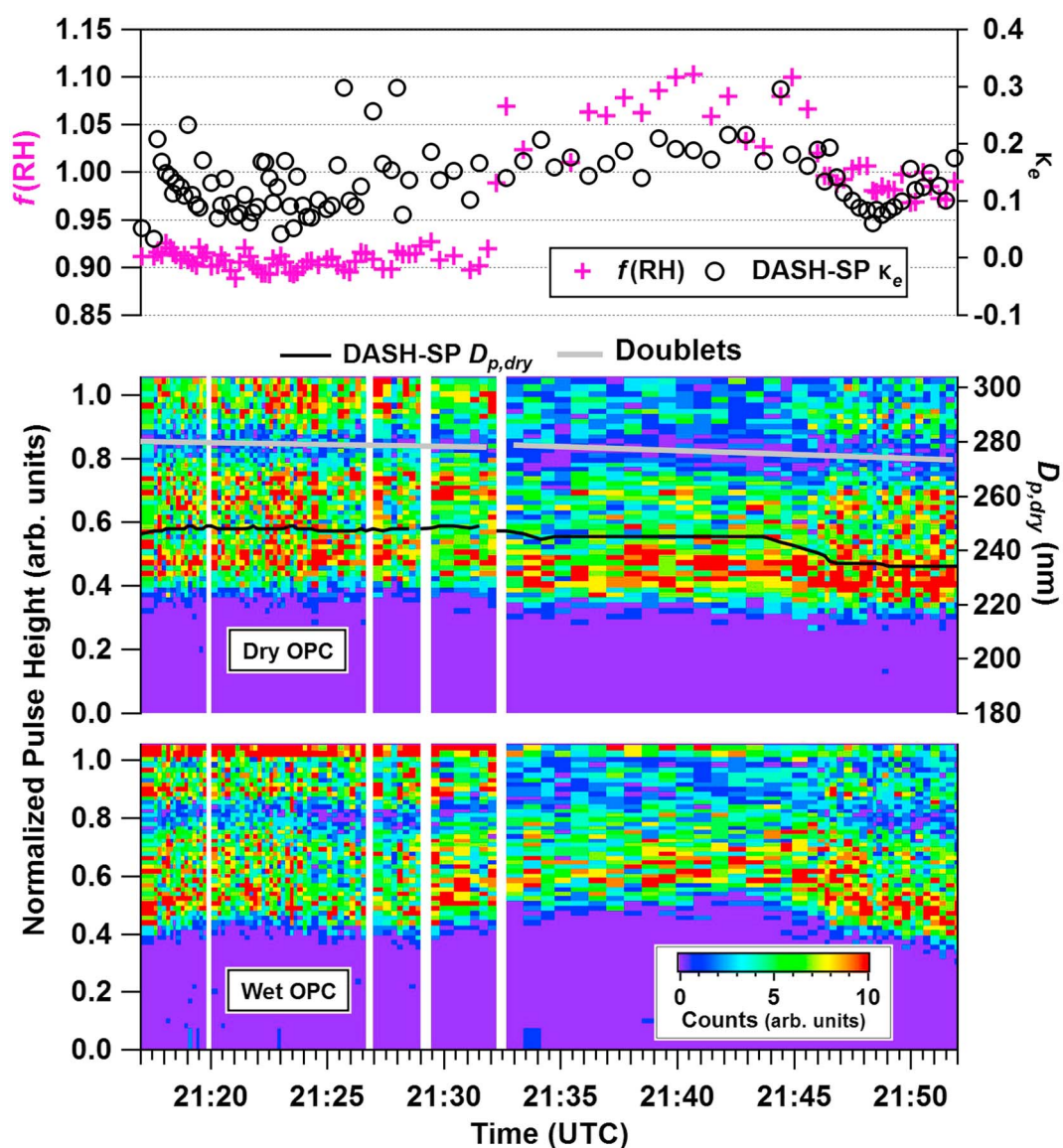


Figure 10. Time series of DASH-SP normalized pulse height distributions for dry and humidified OPCs during the SEAC⁴RS 19 August 2013 flight from 21:00 to 22:00, $D_{p,dry}$ (black line), and hygroscopic growth parameters (κ_e derived from GF values for $D_{p,dry}$ values of 180–400 nm, and $f(\text{RH})$). The drawn gray line in the middle panel is intended to distinguish doubly charged particles from the rest of the data underneath.

microscope analysis indicates the start of “melting” of tar ball particle edges, with effective degradation of tar balls and wetting above a RH of 92%, resulting in irreversible morphological changes.

5. Conclusions

Combining hygroscopicity measurements from three different instruments (DASH-SP, nephelometer, and HTDMA) across multiple field projects and observational platforms, this work presents observations of GF and $f(\text{RH}) < 1$ in the ambient environment. Ship-based HTDMA measurements reveal GFs < 1 exclusively when sampling smoke-like particles in the marine boundary layer off the California coast. Ground-based DASH-SP data in Tucson, Arizona, exhibit GFs < 1 exclusively during winter, coincident with widespread residential wood burning. Aircraft-based data for DASH-SP GF and LARGE $f(\text{RH})$ exhibit hygroscopicity values less than 1 exclusively during wildfire biomass burning sampling. Detailed examination of a biomass burning focused flight during SEAC⁴RS shows that $f(\text{RH})$ is less than 1 in smoke plumes where acetonitrile exceeds

380 pptv, with $f(\text{RH})$ leveling off at 0.9. Reduced effective particle density is coincident with the lowest $f(\text{RH})$ values, and the majority of observations below 1 occur when particle density is less than 1.2 g cm^{-3} . This is suggestive of greater particle restructuring potential in periods with $f(\text{RH}) < 1$. Potential explanations for GF and $f(\text{RH})$ values below 1 were discussed including particle restructuring, effective Rl_{dry} modifications, and evaporation of semivolatile species. A new method for identifying more cases of $\text{GF} < 1$ in the DASH-SP, as compared to the previously used data processing algorithm, is introduced involving identification of externally mixed aerosol.

Future work is warranted to continue unraveling the explanation for GF and $f(\text{RH})$ values below 1. To more robustly study at least the restructuring mechanism in future field projects, a prehumidification channel prior to instrument sizing modules is recommended, which can be switched on and off to hydrate and collapse those particles that have the potential to do so. When sampling aerosol types vulnerable to restructuring such as biomass burning smoke, a reasonable hypothesis would be that switching between prehumidified and nonprehumidified channels should result in GF or $f(\text{RH})$ values below 1 only without prehumidification, as seen in laboratory studies by *Martin et al.* [2013]. Lastly, it is noted that while the focus of this study was on values of GF or $f(\text{RH})$ below 1 being a sufficient condition for knowing when mechanisms such as restructuring are important, it is not a necessary condition. GF and $f(\text{RH})$ values above 1 can still undergo restructuring, for example, but it becomes challenging to untangle the mechanisms discussed in this study from concurrent water uptake.

Acknowledgments

All data used can be obtained from the corresponding author. This research was funded by NASA grants NNX12AC10G and NNX14AP75G, and ONR grant N00014-16-1-2567. The development of the DASH-SP instrument was funded by ONR grant N00014-10-1-0811, and HTDMA measurements in E-PEACE were funded by NSF AGS-1008848. T.S. acknowledges support from a NASA Earth and Space Science Fellowship (NNX14AK79H). Acetonitrile measurements during SEAC⁴RS were supported by the Austrian Federal Ministry for Transport, Innovation and Technology (bmvit) through the Austrian Space Applications Programme (ASAP) of the Austrian Research Promotion Agency (FFG). A.W. and T.M. received support from the Visiting Scientist Program at the National Institute of Aerospace (NIA). L.M.R. acknowledges NSF AGS-1048995 for E-PEACE. P.C.J. and J.L.J. were supported by NASA NNX12AC03G and NNX15AT96G. Manabu Shiraiwa and Andreas Zuend are acknowledged for thermokinetic modeling results.

References

- Atmospheric Science Data Center (2015), NASA Airborne Science Data for Atmospheric Composition: SEAC⁴RS, doi:10.5067/Aircraft/SEAC4RS/Aerosol-TraceGas-Cloud. [Available at <http://www-air.larc.nasa.gov/missions/seac4rs/>.]
- Anderson, T. L., and J. A. Ogren (1998), Determining aerosol radiative properties using the TSI 3563 integrating nephelometer, *Aerosol Sci. Technol.*, *29*(1), 57–69, doi:10.1080/02786829808965551.
- Beaver, M. R., R. M. Garland, C. A. Hasenkopf, T. Baynard, A. R. Ravishankara, and M. A. Tolbert (2008), A laboratory investigation of the relative humidity dependence of light extinction by organic compounds from lignin combustion, *Environ. Res. Lett.*, *3*(4), 045003, doi:10.1088/1748-9326/3/4/045003.
- Canagaratna, M. R., et al. (2007), Chemical and microphysical characterization of ambient aerosols with the aerodyne aerosol mass spectrometer, *Mass Spectrom. Rev.*, *26*(2), 185–222, doi:10.1002/mas.20115.
- Chen, H., D. W. Hu, L. Wang, A. Mellouki, and J. M. Chen (2015), Modification in light absorption cross section of laboratory-generated black carbon-brown carbon particles upon surface reaction and hydration, *Atmos. Environ.*, *116*, 253–261.
- Crosbie, E., J. S. Youn, B. Balch, A. Wonschütz, T. Shingler, Z. Wang, W. C. Conant, E. A. Betterton, and A. Sorooshian (2015), On the competition among aerosol number, size and composition in predicting CCN variability: A multi-annual field study in an urbanized desert, *Atmos. Chem. Phys.*, *15*(12), 6943–6958.
- Cubison, M. J., et al. (2011), Effects of aging on organic aerosol from open biomass burning smoke in aircraft and laboratory studies, *Atmos. Chem. Phys.*, *11*(23), 12,049–12,064, doi:10.5194/acp-11-12049-2011.
- de Gouw, J., and C. Warneke (2007), Measurements of volatile organic compounds in the Earth's atmosphere using proton-transfer-reaction mass spectrometry, *Mass Spectrom. Rev.*, *26*(2), 223–257.
- DeCarlo, P. F., et al. (2006), Field-deployable, high-resolution, time-of-flight aerosol mass spectrometer, *Anal. Chem.*, *78*(24), 8281–8289.
- Dennis-Smith, B. J., R. E. H. Miles, and J. P. Reid (2012), Oxidative aging of mixed oleic acid/sodium chloride aerosol particles, *J. Geophys. Res.*, *117*, D20204, doi:10.1029/2012JD018163.
- Dua, S. K., and P. K. Hopke (1996), Hygroscopicity of indoor aerosols and its influence on the deposition of inhaled radon decay products, *Environ. Int.*, *22*, S941–S947.
- Froyd, K. D., S. M. Murphy, D. M. Murphy, J. A. de Gouw, N. C. Eddingsaas, and P. O. Wennberg (2010), Contribution of isoprene-derived organosulfates to free tropospheric aerosol mass, *Proc. Natl. Acad. Sci. U.S.A.*, *107*(50), 21,360–21,365.
- Garland, R. M., A. R. Ravishankara, E. R. Lovejoy, M. A. Tolbert, and T. Baynard (2007), Parameterization for the relative humidity dependence of light extinction: Organic-ammonium sulfate aerosol, *J. Geophys. Res.*, *112*, D19303, doi:10.1029/2006JD008179.
- Ghazi, R., and J. S. Olfert (2013), Coating mass dependence of soot aggregate restructuring due to coatings of oleic acid and dioctyl sebacate, *Aerosol Sci. Technol.*, *47*(2), 192–200.
- Giordano, M. R., and A. Asa-Awuku (2014), Rebuttal to correspondence on "Changes in droplet surface tension affect the observed hygroscopicity of photochemically aged biomass burning aerosol", *Environ. Sci. Technol.*, *48*(3), 2084–2085.
- Giordano, M. R., D. Z. Short, S. Hosseini, W. Lichtenberg, and A. A. Asa-Awuku (2013), Changes in droplet surface tension affect the observed hygroscopicity of photochemically aged biomass burning aerosol, *Environ. Sci. Technol.*, *47*(19), 10,980–10,986.
- Gysel, M., E. Weingartner, and U. Baltensperger (2002), Hygroscopicity of aerosol particles at low temperatures. 2. Theoretical and experimental hygroscopic properties of laboratory generated aerosols, *Environ. Sci. Technol.*, *36*(1), 63–68.
- Hand, J. L., et al. (2005), Optical, physical, and chemical properties of tar balls observed during the Yosemite Aerosol Characterization Study, *J. Geophys. Res.*, *110*, D21210, doi:10.1029/2004JD005728.
- Henning, S., et al. (2012), Hygroscopic growth and droplet activation of soot particles: Uncoated, succinic or sulfuric acid coated, *Atmos. Chem. Phys.*, *12*(10), 4525–4537, doi:10.5194/acp-12-4525-2012.
- Hersey, S. P., A. Sorooshian, S. M. Murphy, R. C. Flagan, and J. H. Seinfeld (2009), Aerosol hygroscopicity in the marine atmosphere: A closure study using high-time-resolution, multiple-RH DASH-SP and size-resolved C-ToF-AMS data, *Atmos. Chem. Phys.*, *9*(7), 2543–2554.
- Hersey, S. P., J. S. Craven, K. A. Schilling, A. R. Metcalf, A. Sorooshian, M. N. Chan, R. C. Flagan, and J. H. Seinfeld (2011), The Pasadena Aerosol Characterization Observatory (PACO): Chemical and physical analysis of the Western Los Angeles basin aerosol, *Atmos. Chem. Phys.*, *11*(15), 7417–7443.

- Hersey, S. P., et al. (2013), Composition and hygroscopicity of the Los Angeles Aerosol: CalNex, *J. Geophys. Res. Atmos.*, *118*, 3016–3036, doi:10.1002/jgrd.50307.
- Hoffer, A., A. Tóth, I. Nyiró-Kósa, M. Pósfai, and A. Gelencsér (2016), Light absorption properties of laboratory-generated tar ball particles, *Atmos. Chem. Phys.*, *16*(1), 239–246, doi:10.5194/acp-16-239-2016.
- Intergovernmental Panel on Climate Change (2013), Summary for Policymakers, in *Climate Change 2013: The Physical Science Basis. Contribution of Working Group I to the Fifth Assessment Report of the Intergovernmental Panel on Climate Change*, edited by T. F. Stocker et al., pp. 1–30, Cambridge Univ. Press, Cambridge, U. K., and New York.
- Jimenez, J. L., R. Bahreini, D. R. Cocker, H. Zhuang, V. Varutbangkul, R. C. Flagan, J. H. Seinfeld, C. D. O'Dowd, and T. Hoffmann (2003), New particle formation from photooxidation of diiodomethane (CH₂I₂), *J. Geophys. Res.*, *108*(D10), 4318, doi:10.1029/2002JD002452.
- Jung, E., B. A. Albrecht, H. H. Jonsson, Y. C. Chen, J. H. Seinfeld, A. Sorooshian, A. R. Metcalf, S. Song, M. Fang, and L. M. Russell (2015), Precipitation effects of giant cloud condensation nuclei artificially introduced into stratocumulus clouds, *Atmos. Chem. Phys.*, *15*(10), 5645–5658.
- Khalizov, A. F., H. Xue, L. Wang, J. Zheng, and R. Zhang (2009), Enhanced light absorption and scattering by carbon soot aerosol internally mixed with sulfuric acid, *J. Phys. Chem. A*, *113*(6), 1066–1074.
- Khalizov, A. F., Y. Lin, C. Qiu, S. Guo, D. Collins, and R. Y. Zhang (2013), Role of OH-initiated oxidation of isoprene in aging of combustion soot, *Environ. Sci. Technol.*, *47*(5), 2254–2263.
- Kim, P. S., et al. (2015), Sources, seasonality, and trends of southeast US aerosol: An integrated analysis of surface, aircraft, and satellite observations with the GEOS-Chem chemical transport model, *Atmos. Chem. Phys.*, *15*(18), 10,411–10,433, doi:10.5194/acp-15-10411-2015.
- Kramer, U., R. Grimalid, and T. Gould (2015), 2014 air quality summary report, Pima County Department of Environmental Quality, Pima County.
- Kreidenweis, S. M., and A. Asa-Awuku (2014), 5.13—Aerosol hygroscopicity: Particle water content and its role in atmospheric processes, in *Treatise on Geochemistry*, 2nd ed., edited by H. D. H. K. Turekian, pp. 331–361, Elsevier, Oxford.
- Lee, S., S. C. Yoon, S. W. Kim, Y. P. Kim, Y. S. Ghim, J. H. Kim, C. H. Kang, Y. J. Kim, L. S. Chang, and S. J. Lee (2012), Spectral dependency of light scattering/absorption and hygroscopicity of pollution and dust aerosols in Northeast Asia, *Atmos. Environ.*, *50*, 246–254.
- Lee, S.-H., D. M. Murphy, D. S. Thomson, and A. M. Middlebrook (2002), Chemical components of single particles measured with Particle Analysis by Laser Mass Spectrometry (PALMS) during the Atlanta SuperSite Project: Focus on organic/sulfate, lead, soot, and mineral particles, *J. Geophys. Res.*, *107*(D1), 4003, doi:10.1029/2000JD000011.
- Lewis, K. A., et al. (2009), Reduction in biomass burning aerosol light absorption upon humidification: Roles of inorganically-induced hygroscopicity, particle collapse, and photoacoustic heat and mass transfer, *Atmos. Chem. Phys.*, *9*(22), 8949–8966.
- Liu, B. Y. H. (1978), Aerosol instrumentation—Generation, standards, measurement techniques, and data reduction, *Staub Reinhalt. Luft*, *38*(2), 43–45.
- Lopez-Yglesias, X. F., M. C. Yeung, S. E. Dey, F. J. Brechtel, and C. K. Chan (2014), Performance evaluation of the Brechtel Mfg. humidified tandem differential mobility analyzer (BMI HTDMA) for studying hygroscopic properties of aerosol particles, *Aerosol Sci. Technol.*, *48*(9), 969–980.
- Ma, X. F., C. D. Zangmeister, J. Gigault, G. W. Mulholland, and M. R. Zachariah (2013), Soot aggregate restructuring during water processing, *J. Aerosol Sci.*, *66*, 209–219.
- Malm, W. C., D. E. Day, C. Carrico, S. M. Kreidenweis, J. L. Collett Jr., G. McMeeking, T. Lee, J. Carrillo, and B. Schichtel (2005), Intercomparison and closure calculations using measurements of aerosol species and optical properties during the Yosemite Aerosol Characterization Study, *J. Geophys. Res.*, *110*, D14302, doi:10.1029/2004JD005494.
- Martin, M., et al. (2013), Hygroscopic properties of fresh and aged wood burning particles, *J. Aerosol Sci.*, *56*, 15–29, doi:10.1016/j.jaerosci.2012.08.006.
- McNaughton, C. S., et al. (2007), Results from the DC-8 Inlet Characterization Experiment (DICE): Airborne versus surface sampling of mineral dust and sea salt aerosols, *Aerosol Sci. Technol.*, *41*(2), 136–159, doi:10.1080/02786820601118406.
- Mikhailov, E., S. Vlasenko, R. Niessner, and U. Pöschl (2004), Interaction of aerosol particles composed of protein and salts with water vapor: Hygroscopic growth and microstructural rearrangement, *Atmos. Chem. Phys.*, *4*(2), 323–350.
- Mikhailov, E., S. Vlasenko, S. T. Martin, T. Koop, and U. Pöschl (2009), Amorphous and crystalline aerosol particles interacting with water vapor: Conceptual framework and experimental evidence for restructuring, phase transitions and kinetic limitations, *Atmos. Chem. Phys.*, *9*(24), 9491–9522.
- Mikhailov, E. F., S. S. Vlasenko, I. A. Podgorny, V. Ramanathan, and C. E. Corrigan (2006), Optical properties of soot-water drop agglomerates: An experimental study, *J. Geophys. Res.*, *111*, D07209, doi:10.1029/2005JD006389.
- Mochida, M., and K. Kawamura (2004), Hygroscopic properties of levoglucosan and related organic compounds characteristic to biomass burning aerosol particles, *J. Geophys. Res.*, *109*, D21202, doi:10.1029/2004JD004962.
- Modini, R. L., et al. (2015), Primary marine aerosol-cloud interactions off the coast of California, *J. Geophys. Res. Atmos.*, *120*, 4282–4303, doi:10.1002/2014JD022963.
- Montgomery, J. F., S. N. Rogak, S. I. Green, Y. You, and A. K. Bertram (2015), Structural change of aerosol particle aggregates with exposure to elevated relative humidity, *Environ. Sci. Technol.*, *49*(20), 12,054–12,061.
- Onischuk, A. A., S. di Stasio, V. V. Karasev, A. M. Baklanov, G. A. Makhov, A. L. Vlasenko, A. R. Sadykova, A. V. Shipovalov, and V. N. Panfilov (2003), Evolution of structure and charge of soot aggregates during and after formation in a propane/air diffusion flame, *J. Aerosol Sci.*, *34*(4), 383–403.
- Pagels, J., A. F. Khalizov, P. H. McMurry, and R. Y. Zhang (2009), Processing of soot by controlled sulphuric acid and water condensation mass and mobility relationship, *Aerosol Sci. Technol.*, *43*(7), 629–640.
- Perring, A. E., et al. (2016), In-situ measurements of water uptake by black carbon-containing aerosol in wildfire plumes, *J. Geophys. Res. Atmos.*, submitted.
- Petters, M. D., and S. M. Kreidenweis (2007), A single parameter representation of hygroscopic growth and cloud condensation nucleus activity, *Atmos. Chem. Phys.*, *7*(8), 1961–1971.
- Petters, M. D., and S. M. Kreidenweis (2008), A single parameter representation of hygroscopic growth and cloud condensation nucleus activity—Part 2: Including solubility, *Atmos. Chem. Phys.*, *8*(20), 6273–6279.
- Petters, M. D., and S. M. Kreidenweis (2013), A single parameter representation of hygroscopic growth and cloud condensation nucleus activity—Part 3: Including surfactant partitioning, *Atmos. Chem. Phys.*, *13*(2), 1081–1091.
- Posfai, M., A. Gelencsér, R. Simonics, K. Arato, J. Li, P. V. Hobbs, and P. R. Buseck (2004), Atmospheric tar balls: Particles from biomass and biofuel burning, *J. Geophys. Res.*, *109*, D06213, doi:10.1029/2003JD004169.

- Rader, D. J., and P. H. McMurry (1986), Application of the tandem differential mobility analyzer to studies of droplet growth or evaporation, *J. Aerosol Sci.*, *17*(5), 771–787.
- Rissler, J., J. Pagels, E. Swietlicki, A. Wierzbicka, M. Strand, L. Lillieblad, M. Sanati, and M. Bohgard (2005), Hygroscopic behavior of aerosol particles emitted from biomass fired grate boilers, *Aerosol Sci. Technol.*, *39*(10), 919–930.
- Russell, L. M., et al. (2013), Eastern pacific emitted aerosol cloud experiment, *Bull. Am. Meteorol. Soc.*, *94*(5), 709–729, doi:10.1175/BAMS-D-12-00015.1.
- Saide, P. E., et al. (2015), Revealing important nocturnal and day-to-day variations in fire smoke emissions through a multiplatform inversion, *Geophys. Res. Lett.*, *42*, 3609–3618, doi:10.1002/2015GL063737.
- Sanchez, K. J., et al. (2016), Meteorological and aerosol effects on marine cloud microphysical properties, *J. Geophys. Res. Atmos.*, *121*, 4142–4161, doi:10.1002/2015JD024595.
- Schnitzler, E. G., A. Dutt, A. M. Charbonneau, J. S. Olfert, and W. Jager (2014), Soot aggregate restructuring due to coatings of secondary organic aerosol derived from aromatic precursors, *Environ. Sci. Technol.*, *48*(24), 14,309–14,316.
- Schwarz, J. P., A. E. Perring, M. Z. Markovic, R. S. Gao, S. Ohata, J. Langridge, D. Law, R. McLaughlin, and D. W. Fahey (2015), Technique and theoretical approach for quantifying the hygroscopicity of black-carbon-containing aerosol using a single particle soot photometer, *J. Aerosol Sci.*, *81*, 110–126.
- Shingler, T., et al. (2016), Airborne characterization of sub-saturated aerosol hygroscopicity and dry refractive index from the surface to 6.5 km during the SEAC⁴RS campaign, *J. Geophys. Res. Atmos.*, *121*, 4188–4210, doi:10.1002/2015JD024498.
- Shiraiwa, M., C. Pfrang, T. Koop, and U. Poschl (2012), Kinetic multi-layer model of gas-particle interactions in aerosols and clouds (KM-GAP): Linking condensation, evaporation and chemical reactions of organics, oxidants and water, *Atmos. Chem. Phys.*, *12*(5), 2777–2794.
- Sorooshian, A., S. Hersey, F. J. Brechtel, A. Corless, R. C. Flagan, and J. H. Seinfeld (2008a), Rapid, size-resolved aerosol hygroscopic growth measurements: Differential Aerosol Sizing and Hygroscopicity Spectrometer Probe (DASH-SP), *Aerosol Sci. Technol.*, *42*(6), 445–464.
- Sorooshian, A., S. N. Murphy, S. Hersey, H. Gates, L. T. Padro, A. Nenes, F. J. Brechtel, H. Jonsson, R. C. Flagan, and J. H. Seinfeld (2008b), Comprehensive airborne characterization of aerosol from a major bovine source, *Atmos. Chem. Phys.*, *8*(17), 5489–5520.
- Sorooshian, A., E. Crosbie, L. C. Maudlin, J.-S. Youn, Z. Wang, T. Shingler, A. M. Ortega, S. Hersey, and R. K. Woods (2015), Surface and airborne measurements of organosulfur and methanesulfonate over the western United States and coastal areas, *J. Geophys. Res. Atmos.*, *120*, 8535–8548, doi:10.1002/2015JD023822.
- Toon, O. B., et al. (2016), Planning, implementation, and scientific goals of the Studies of Emissions and Atmospheric Composition, Clouds and Climate Coupling by Regional Surveys (SEAC⁴RS) field mission, *J. Geophys. Res. Atmos.*, *121*, 4967–5009, doi:10.1002/2015JD024297.
- Tritscher, T., et al. (2011), Volatility and hygroscopicity of aging secondary organic aerosol in a smog chamber, *Atmos. Chem. Phys.*, *11*(22), 11,477–11,496, doi:10.5194/acp-11-11477-2011.
- U.S. Census Bureau (2011), [Available at <http://www.census.gov/popest/data/index.html>.]
- Wang, Z., A. Sorooshian, G. Prabhakar, M. M. Coggon, and H. H. Jonsson (2014), Impact of emissions from shipping, land, and the ocean on stratocumulus cloud water elemental composition during the 2011 E-PEACE field campaign, *Atmos. Environ.*, *89*, 570–580.
- Weingartner, E., U. Baltensperger, and H. Burtscher (1995), Growth and structural-change of combustion aerosols at high relative-humidity, *Environ. Sci. Technol.*, *29*(12), 2982–2986.
- Weingartner, E., H. Burtscher, and U. Baltensperger (1997), Hygroscopic properties of carbon and diesel soot particles, *Atmos. Environ.*, *31*(15), 2311–2327.
- Wonaschütz, A., et al. (2013), Hygroscopic properties of smoke-generated organic aerosol particles emitted in the marine atmosphere, *Atmos. Chem. Phys.*, *13*(19), 9819–9835, doi:10.5194/acp-13-9819-2013.
- Xue, H. X., A. F. Khalizov, L. Wang, J. Zheng, and R. Y. Zhang (2009), Effects of coating of dicarboxylic acids on the mass-mobility relationship of soot particles, *Environ. Sci. Technol.*, *43*(8), 2787–2792.
- Youn, J.-S., Z. Wang, A. Wonaschütz, A. Arellano, E. A. Betterton, and A. Sorooshian (2013), Evidence of aqueous secondary organic aerosol formation from biogenic emissions in the North American Sonoran Desert, *Geophys. Res. Lett.*, *40*, 3468–3472, doi:10.1002/grl.50644.
- Youn, J. S., E. Crosbie, L. C. Maudlin, Z. Wang, and A. Sorooshian (2015), Dimethylamine as a major alkyl amine species in particles and cloud water: Observations in semi-arid and coastal regions, *Atmos. Environ.*, *122*, 250–258.
- Zhang, R. Y., A. F. Khalizov, J. Pagels, D. Zhang, H. X. Xue, and P. H. McMurry (2008), Variability in morphology, hygroscopicity, and optical properties of soot aerosols during atmospheric processing, *Proc. Natl. Acad. Sci. U.S.A.*, *105*(30), 10,291–10,296.
- Ziemba, L. D., et al. (2013), Airborne observations of aerosol extinction by in situ and remote-sensing techniques: Evaluation of particle hygroscopicity, *Geophys. Res. Lett.*, *40*, 417–422, doi:10.1029/2012GL054428.
- Zuend, A., C. Marcolli, B. P. Luo, and T. Peter (2008), A thermodynamic model of mixed organic-inorganic aerosols to predict activity coefficients, *Atmos. Chem. Phys.*, *8*(16), 4559–4593.
- Zuend, A., C. Marcolli, A. M. Booth, D. M. Lienhard, V. Soonsin, U. K. Krieger, D. O. Topping, G. McFiggans, T. Peter, and J. H. Seinfeld (2011), New and extended parameterization of the thermodynamic model AIOMFAC: Calculation of activity coefficients for organic-inorganic mixtures containing carboxyl, hydroxyl, carbonyl, ether, ester, alkenyl, alkyl, and aromatic functional groups, *Atmos. Chem. Phys.*, *11*(17), 9155–9206.